J Neurophysiol 112: 2470–2480, 2014.
First published August 13, 2014; doi:10.1152/jn.00410.2014.

Visual selectivity for heading in the macaque ventral intraparietal area

Andre Kaminiarz,[1] Anja Schlack,[2] Klaus-Peter Hoffmann,[1,2] Markus Lappe,[3] and Frank Bremmer[1]
[1]*AG Neurophysik, University of Marburg, Marburg, Germany;* [2]*Allgemeine Zoologie und Neurobiologie, University of Bochum, Bochum, Germany; and* [3]*Institut für Psychologie, University of Münster, Münster, Germany*

Submitted 2 June 2014; accepted in final form 11 August 2014

Kaminiarz A, Schlack A, Hoffmann KP, Lappe M, Bremmer F. Visual selectivity for heading in the macaque ventral intraparietal area. *J Neurophysiol* 112: 2470–2480, 2014. First published August 13, 2014; doi:10.1152/jn.00410.2014.—The patterns of optic flow seen during self-motion can be used to determine the direction of one's own heading. Tracking eye movements which typically occur during everyday life alter this task since they add further retinal image motion and (predictably) distort the retinal flow pattern. Humans employ both visual and nonvisual (extraretinal) information to solve a heading task in such case. Likewise, it has been shown that neurons in the monkey medial superior temporal area (area MST) use both signals during the processing of self-motion information. In this article we report that neurons in the macaque ventral intraparietal area (area VIP) use visual information derived from the distorted flow patterns to encode heading during (simulated) eye movements. We recorded responses of VIP neurons to simple radial flow fields and to distorted flow fields that simulated self-motion plus eye movements. In 59% of the cases, cell responses compensated for the distortion and kept the same heading selectivity irrespective of different simulated eye movements. In addition, response modulations during real compared with simulated eye movements were smaller, being consistent with reafferent signaling involved in the processing of the visual consequences of eye movements in area VIP. We conclude that the motion selectivities found in area VIP, like those in area MST, provide a way to successfully analyze and use flow fields during self-motion and simultaneous tracking movements.

self-motion; primate; parietal cortex; eye movements

SELF-MOTION THROUGH AN ENVIRONMENT induces visual, vestibular, tactile, and auditory signals. Neurophysiological research over the last two decades has shown in the animal model, i.e., the macaque monkey, how these signals interact to enhance and disambiguate the perception of heading during self-motion. Two areas of the primate extrastriate and parietal cortex proved to be of specific importance in this context, i.e., the medial superior temporal area (area MST) and the ventral intraparietal area (area VIP). Neurons in area MST respond to visual and vestibular self-motion signals, and their causal role in heading perception has been confirmed (Bremmer et al. 1999; Duffy 1998; Duffy and Wurtz 1991a, 1991b; Gu et al. 2007, 2008, 2010, 2012; Lappe et al. 1996; Morgan et al. 2008; Page and Duffy 2003; Yu et al. 2010). Neurons in area VIP respond not only to visual and vestibular but also to tactile and auditory stimulation (Avillac et al. 2005, 2007; Ben Hamed et al. 2002; Bremmer et al. 2002a, 2002b; Chen et al. 2011b; Duhamel et al. 1998; Schlack et al. 2002). Like for area MST, behavioral experiments have demonstrated a critical role of area VIP for heading perception (Britten 2008; Chen et al. 2013; Zhang et al. 2004; Zhang and Britten 2011).

Neurons in area MST integrate visual and vestibular self-motion signals with extraretinal eye-movement information to dissociate self-induced motion from external motion (Bradley et al. 1996; Shenoy et al. 1999; Upadhyay et al. 2000). Such multisensory convergence of self-motion signals is clearly suited to improve heading. Nevertheless, perceptual performance could be further enhanced if single neurons were capable of deducing heading information from visual signals alone. Accordingly, we recently reported that neurons in area MST can encode heading solely based on visual signals (Bremmer et al. 2010). Such neurons kept their heading selectivity regardless of whether or not the retinal flow resulting from a simulated forward motion was disturbed by superimposed simulated eye movements of various gains.

Area VIP shares a number of functional properties with area MST (Colby et al. 1993). Most importantly, many VIP neurons, like those in area MST, respond strongly to visual stimuli simulating self-motion (e.g., Bremmer et al. 2002a; Britten 2008; Chen et al. 2011a, 2013). In our current study, we asked whether also neurons from area VIP reveal an invariance of their heading selectivity with respect to simulated and/or real tracking eye movements. We tested VIP neurons for their responses to simple radial flow fields and to distorted flow fields that simulated an eye movement during self-motion. In 59% of the cases, cell responses compensated for such distortion and kept the same heading selectivity irrespective of the simulated eye movement. Remarkably, response modulations, i.e., differences between the strongest and the weakest heading response for a given eye-movement condition, were smaller during real compared with simulated eye movements. This latter finding might be due to reafferent signals, which modulate the processing of visual self-motion information in area VIP. Taken together, our results strongly support the notion of an involvement of area VIP in visual navigation.

MATERIALS AND METHODS

Animal preparation. Single-unit recordings were performed in two awake, behaving monkeys (*Macaca mulatta*). All procedures were in accordance with published guidelines on the use of animals in research (European Communities Council Directive 86/609/ECC). Experimental methods followed standard procedures that are described in more detail in (Bremmer et al. 2009) and (Morris et al. 2012). In brief, monkeys were surgically prepared for chronic neurophysiological recordings in area VIP. Under general anesthesia and sterile surgical conditions each animal was implanted with a device for holding the head and scleral search coils for eye position monitoring (Judge et al. 1980). A recording chamber for microelectrode penetrations through the intact dura was placed in a frontal plane at an angle

Address for reprint requests and other correspondence: F. Bremmer, Dept. of Neurophysics, Univ. of Marburg, Karl-v-Frisch Str. 8a, D-35043 Marburg, Germany (e-mail: frank.bremmer@physik.uni-marburg.de).

of 45° with respect to the vertical for recordings in area VIP. In both monkeys, the exact location of the craniotomy was determined on the basis of presurgical MR scanning. Recording chamber, eye coil plugs, and head holders were embedded in a dental acrylic cap, which itself was connected to the skull by self-tapping screws. Analgesics were applied postoperatively, and recording started no sooner than 1 wk after surgery.

Behavioral paradigm and recordings. Before the experiments, monkeys were trained on a fixation task. During training and recording sessions, the monkey's head was restrained on a primate chair while the monkey was either performing a fixation task or was allowed to freely move its eyes. In trials that required fixation, the target was always presented in the center of the screen, and the monkey had to maintain central fixation within an electronically controlled window (2° diameter) throughout the trial. Horizontal and vertical eye position were monitored with a search coil (Robinson 1963) and sampled at 500 Hz. Single-unit activity was recorded using tungsten-in-glass electrodes and a hydraulic microdrive (Narishige, London, UK). In some experiments a multielectrode recording system (Thomas Recording, Giessen, Germany) was used. In both cases, an online spike sorting system (MSD; Alpha Omega, Ubstadt-Weiher, Germany) was used to isolate multiple single-unit data from a single electrode. Behavioral paradigm, visual stimulation, and data acquisition were controlled by a personal computer and custom-made software. At the end of the training or experimental sessions, the monkey was returned to its home cage. The monkey's weight was monitored daily, and supplementary fruit or water supply was provided if necessary.

Optic flow stimuli were generated in OpenGL with a frame rate of 72 Hz. The stimuli consisted of large-field computer-generated sequences that were back-projected via a video projector (Electrohome) onto a tangent screen 48 cm in front of the monkey. The size of the projection covered the central 90° × 90° of the visual field. Optic flow sequences simulated self-motion of a virtual observer over an extended horizontal plane covered with a texture pattern and located 37 cm below eye level. Trials simulated self-motion at 1 m/s in one of three directions: 30° to the left, straight ahead, and 30° to the right. These three different self-motion directions were combined with three different gains (G) of simulated eye movements: gain = 0.0 (fixed gaze), gain = 0.5 (aiming at the natural viewing behavior as indicated by Lappe et al. 1998), and gain = 1.0 (imitating perfect tracking of a stationary target on the ground plane). These $3 \times 3 = 9$ different stimulus conditions were presented in pseudorandomized order across trials and were combined with blocks of trials during which the animal was allowed to perform spontaneous, unrestrained eye movements. Here, the same three different self-motion directions as in the simulated eye-movement condition were presented in pseudorandomized order across trials.

Data analysis. Neural activity and eye movements were analyzed using custom-made software running under MATLAB (The MathWorks). In a first step, we determined those neurons whose stimulus-induced response was significantly different from baseline activity as obtained during fixation of a central target and a stationary ground-plane pattern. To this end, we employed a nonparametric approach (ANOVA on ranks) rather than a parametric one, since discharges cannot be distributed normally. This is due to the fact that in a strict mathematical sense, a normal distribution would require also negative values. Neuronal firing rates, however, cannot be negative. Differences in discharges resulting in $P < 0.05$ were considered statistically significant. For this subgroup of neurons, activity for all simulated eye-movement gains was determined in a fixed response window, i.e., for the whole self-motion duration (2,500 ms), shifted by an estimated response latency of 100 ms. For a given eye-movement condition, these average responses were ranked according to each neuron's response for each self-motion direction. As an example, assume a neuron showed its largest response for rightward motion for simulated gain = 0.0. Accordingly, its rank = ⟨1⟩. We then determined its rank for rightward movement for the other two simulated eye-movement conditions. If the response was highest for rightward movement, irrespective of the simulated eye movement, the rank-order triplet was ⟨1-1-1⟩. If, at the same time, the second largest response was obtained for straight-ahead motion for all eye-movement conditions, this resulted in a rank-order triplet ⟨2-2-2⟩. This, in turn, implied that the weakest responses were obtained for simulated leftward motion, resulting in a rank-order triplet ⟨3-3-3⟩. In summary, the response of each neuron resulted in three rank-order triplets, one for each self-motion direction. The total number of rank-order triplets was therefore three times the number of neurons with a significant stimulus-induced response. This analysis did not consider, however, the eye-movement condition (gain) for which a given rank was obtained: as an example, rank orders ⟨1-1-2⟩, ⟨1-2-1⟩, and ⟨2-1-1⟩ were considered to be identical. Our analysis therefore led to a total of 10 possible rank-order triplets: ⟨1-1-1⟩, ⟨2-2-2⟩, ⟨3-3-3⟩, ⟨1-1-2⟩, ⟨1-1-3⟩, ⟨1-2-2⟩, ⟨1-3-3⟩, ⟨2-2-3⟩, ⟨2-3-3⟩, and ⟨1-2-3⟩. From a statistical point of view, rank-order triplets ⟨1-1-1⟩, ⟨2-2-2⟩, and ⟨3-3-3⟩ could occur most rarely (each of them only in 1 of $3^3 = 27$ cases), whereas, from a theoretical point of view, the rank-order triplet ⟨1-2-3⟩ could occur most often (in 6 of 27 cases). We employed a χ^2 or a Fisher exact test ($P < 0.05$) to determine whether the proportion of rank-order triplets found in our recordings differed from a random distribution that was to be expected if heading responses across eye-movement conditions were unrelated.

In the free eye-movement condition, saccades were detected by an eye-velocity criterion (threshold set to V_{th} = 80 deg/s). Tracking phases in which eye position was outside the central ± 10 by ± 10° of the screen were excluded from further analysis to avoid possible contamination of neural activity by eye position signals or visually induced screen-border effects. From the remaining data set, all tracking phases were temporally aligned to the offset of the preceding fast eye movement. Average neural activity was determined across these tracking phases for each of the three self-motion directions.

RESULTS

We recorded from 68 VIP neurons of 2 awake, behaving monkeys (*monkey H*: left hemisphere, 45 neurons; *monkey C*: right hemisphere, 23 neurons) during simulated self-motion in 3 different directions (straight ahead or 30° to the left or right) over a virtual horizontal plane 37 cm below eye level. In blocks of trials, in which the animals always fixated a central target, each of the three simulated self-translations were combined with three simulated eye-movement behaviors: eye rotation with *1*) gain = 0.5 or *2*) gain = 1.0, or *3*) fixation (gain = 0.0). The resulting $3 \times 3 = 9$ different retinal flow patterns are shown schematically in Fig. 1. In each panel, the arrow indicates the direction of self-motion, whereas the circle indicates the monkeys' fixation location. As shown in the *top* row (gain = 0.0), self-motion with fixed gaze induces a flow pattern with a singularity being indicative of one's heading direction (Gibson 1950). Furthermore, a characteristic spiraling motion pattern occurs when (real or simulated) tracking eye movements (gain = 0.5 or 1.0) are added to the self-translation (Lappe and Rauschecker 1994; Warren and Hannon 1988).

VIP neurons are tuned to the location of the singularity of the optic flow (Bremmer et al. 2002a). Accordingly, the condition with simulated fixed gaze served as a reference for each neuron's heading sensitivity. Forty-eight of 68 neurons (71%) showed a significant stimulus response [ANOVA on ranks, 9 degrees of freedom (df), $P < 0.05$], 30/45 neurons (67%) in *monkey H* and 18/23 neurons (78%) in *monkey C*. An example response is shown in the *top* row of Fig. 2 (gain = 0.0). This

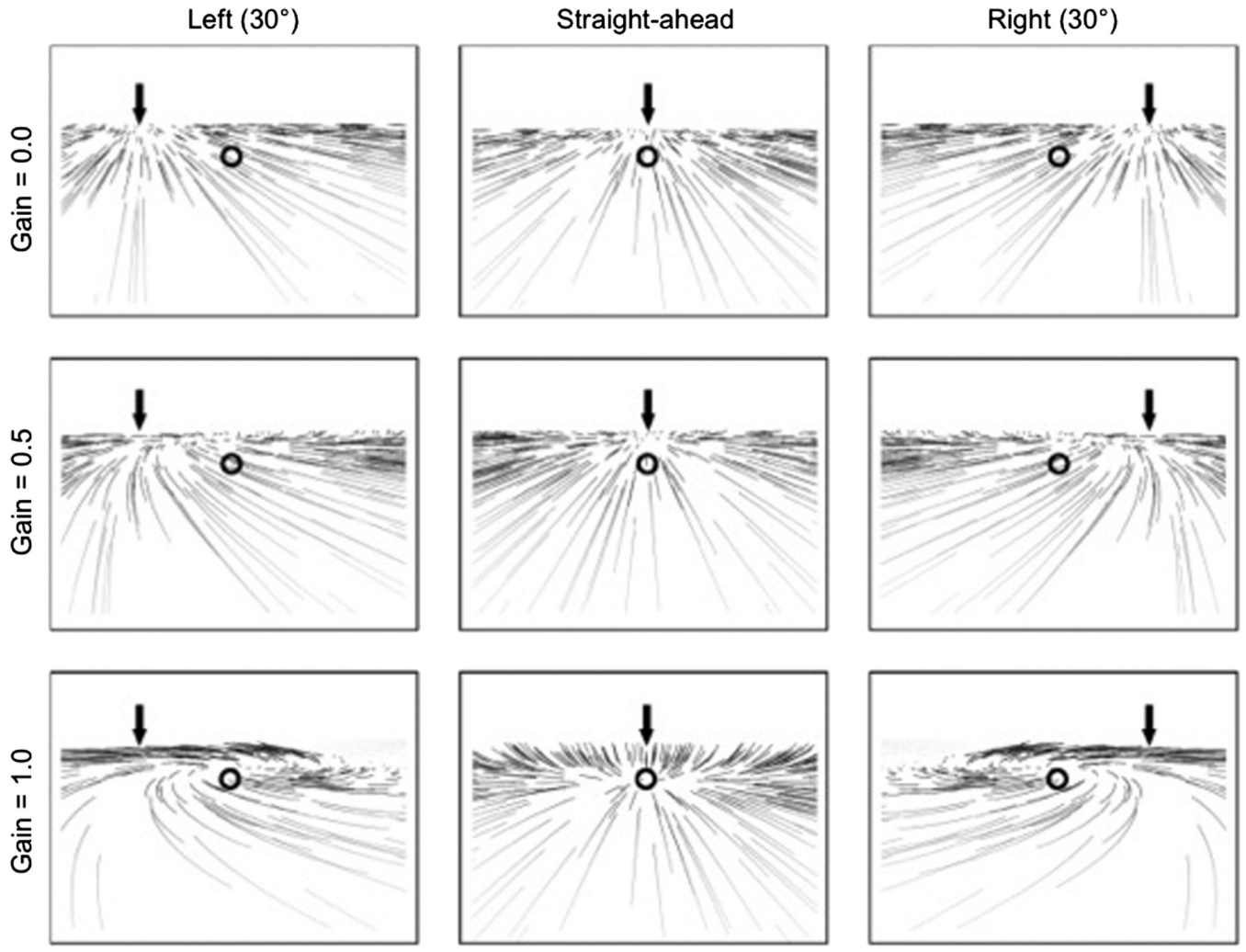

Fig. 1. Retinal flow fields seen by an observer moving over a ground plane. Stimuli were back-projected onto a large tangent screen and covered the central 90° × 90° of the visual field. Each panel illustrates one of the resulting optic flow stimuli. Panels in *left*, *middle*, and *right* columns each display the same heading (arrow) but differ in terms of eye movements. Accordingly, panels in *top*, *middle*, and *bottom* rows display the same eye-movement condition (gain) but differ in terms of heading. Simulated self-motion was 30° to the left or right and straight ahead. Simulated eye movements could have various gain values. Gain = 0.0 simulates steady fixation. Gain = 0.5 simulates a reflexive eye movement occurring under natural viewing conditions (Lappe et al. 1998). Gain = 1.0 mimics tracking of a stationary target on the ground. Monkeys had to fixate a central target (circle) in all cases.

neuron was significantly tuned for leftward heading (ANOVA on ranks, 2 df, $P < 0.001$; a Tukey pairwise comparison was significant in all 3 cases, i.e., left vs. right, left vs. straight ahead, straight ahead vs. right: $P < 0.05$). Simulated heading to the right resulted in a significant drop of discharge below baseline activity (Mann-Whitney rank test, $P < 0.001$).

The other two simulated eye-movement conditions distorted the retinal flow pattern but kept the simulated heading intact. One condition simulated perfect tracking with gain = 1.0, which corresponds to a situation where the animal actively tracks a stationary element on the ground (stimulus: Fig. 1, *bottom* row; example response: Fig. 2, *bottom* row). The other condition simulated the typical behavior during spontaneous eye movements, i.e., tracking with gain = 0.5 (Lappe et al. 1998; stimulus: Fig. 1, *middle* row; example response: Fig. 2, *middle* row). As can be easily seen from Fig. 2, the tuning of the neuron's response for simulated self-motion was unaffected by the different simulated eye movements. In all cases, the neuron preferred leftward over straight-ahead heading, and this in turn was preferred over rightward heading. Responses for a given heading direction (left, straight ahead, or right) were not significantly different for the three eye-movement conditions (ANOVAs on ranks, 2 df: left, $P > 0.06$; straight ahead, $P > 0.9$; right, $P > 0.06$).

To further quantify the neuronal responses, we ranked the response strength of each individual neuron as determined from a fixed-response window (complete stimulation duration, shifted by an estimated response latency of 100 ms, i.e., 100 to 2,600 ms after self-motion onset) for each simulated eye-movement condition (gain = 0.0, 0.5, and 1.0). This procedure can be illustrated based on the example response shown in Fig. 2. Average discharges per condition are given in each histogram panel of Fig. 2. As discussed above, discharges in the "no eye movement" condition (gain = 0.0; *top* row) were strongest for leftward heading (rank = 1), medium for straight-ahead movement (rank = 2), and lowest for rightward heading (rank = 3). The same ranking was found for the other two eye-movement conditions. Hence, the rank-order triplets across the three different eye-movement conditions for leftward, straight-ahead, and rightward self-motion as obtained from the

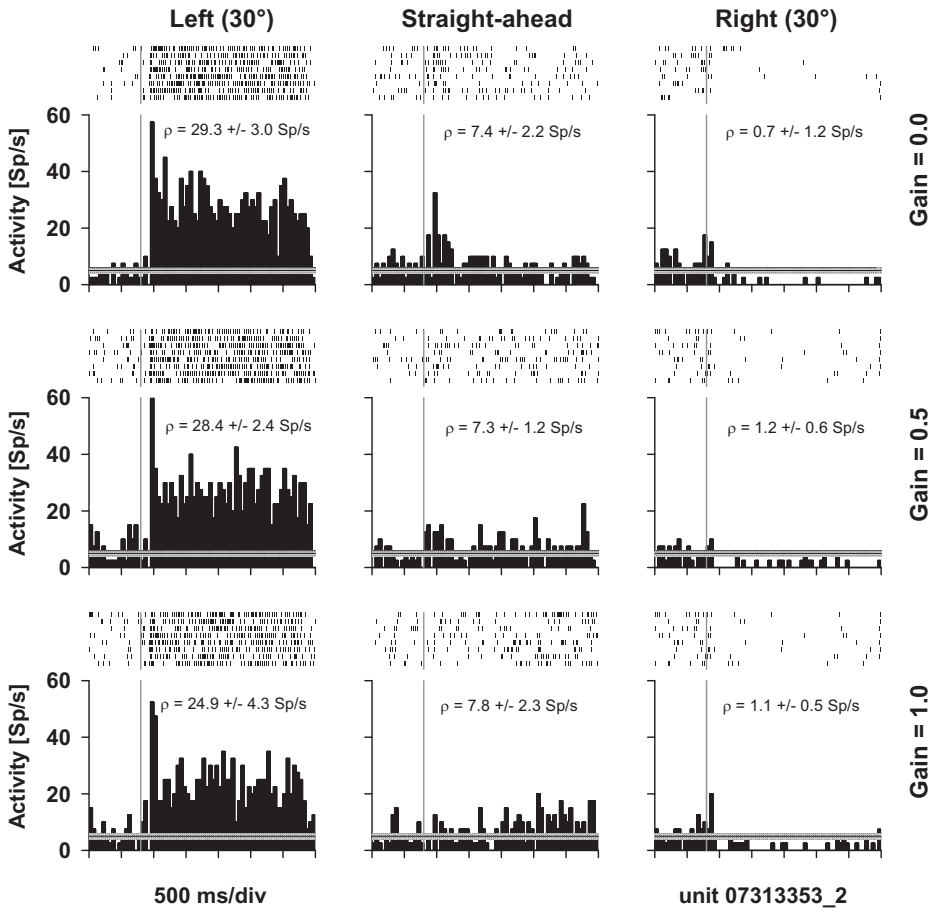

Fig. 2. Responses from a neuron responding to leftward heading irrespective of simulated eye movements. Histograms show the neuron's firing rate over time (Sp/s, spikes/s) during presentation of the optic flow stimuli as indicated in Fig. 1. ρ values in each panel indicate the average discharge ($\pm$SD). The horizontal thin black line in each histogram indicates the median of baseline activity. The horizontal gray bar surrounding the black line illustrates the 95% confidence interval of this median baseline activity. Raster displays above each histogram show occurrence of spikes in all individual trials. Gray vertical lines indicate onset of simulated self-motion. Panels in *left*, *middle*, and *right* columns represent responses to leftward, straight-ahead, and rightward heading stimuli, respectively, for different eye movement conditions. In all cases, the animal continuously fixated a central target. Irrespective of the simulated eye-movement condition, the neuron's strongest response was observed during leftward heading. Forward heading resulted in a medium response. A drop of activity below spontaneous discharge (Mann-Whitney rank test, $P < 0.05$) was induced by rightward heading.

responses of this neuron were ⟨1-1-1⟩ (leftward), ⟨2-2-2⟩ (straight-ahead), and ⟨3-3-3⟩ (rightward), respectively.

For a given heading direction, this ranking procedure could result in $3 \times 3 \times 3 = 27$ different outcomes. Three of them were unique (⟨1-1-1⟩, ⟨2-2-2⟩, and ⟨3-3-3⟩), corresponding to an expected frequency of $(1/27) \times 100\% = 3.7\%$ for each of these three rank-order triplets (see MATERIALS AND METHODS for details). Figure 3 shows the distribution of these rank-order triplets and the expected proportions as obtained from the population of neurons with a significant stimulus response. Given data from 30 neurons in *monkey H* and from 18 neurons in *monkey C*, this resulted in a total of $n = (30 \times 3) + (18 \times 3) = 144$ cases. Peak discharges for identical heading directions (i.e., rank-order triplet ⟨1-1-1⟩) were observed in $32/144 = 22\%$ of the cases. Weakest discharges for identical heading (⟨3-3-3⟩) occurred in $29/144 = 20\%$ of the cases, and medium discharges for identical heading (⟨2-2-2⟩) occurred in $24/144 = 17\%$ of the cases. Each of these individual rank-order triplets indicates the invariance of a neuron's heading response with respect to simulated eye movements. Accordingly, such invari-

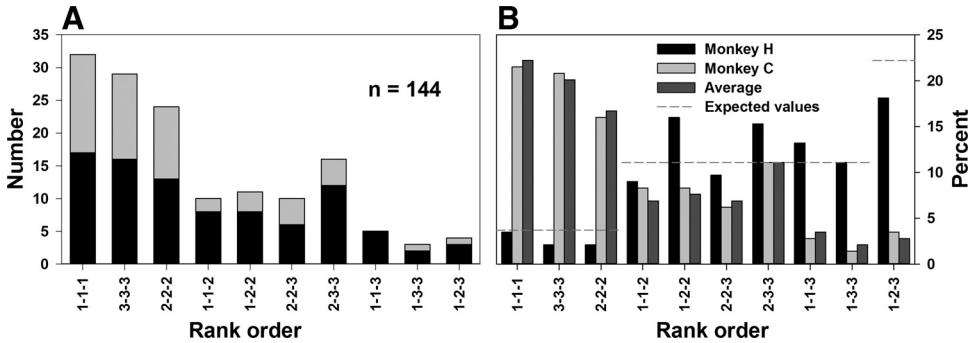

Fig. 3. Distribution of rank-order triplets. For each cell, we ranked (from ⟨1⟩ = strongest to ⟨3⟩ = weakest) for each simulated self-motion direction the responses of a neuron for each of the 3 simulated eye-movement conditions. As an example: responses for leftward self-motion as shown in Fig. 2 were strongest for gain = 1.0, 0.5, and 0.0, resulting in a rank-order triplet ⟨1-1-1⟩. Responses for rightward self-motion were always weakest (rank-order triplet ⟨3-3-3⟩, and responses for straight-ahead self-motion were always medium (⟨2-2-2⟩). This analysis therefore led to a total of 10 possible rank-order triplets. *A* shows the absolute number of each of the rank-order triplets for both monkeys. *B* shows the resulting proportions, for each monkey and as an average. From a statistical point of view, rank-order triplets ⟨1-1-1⟩, ⟨2-2-2⟩, and ⟨3-3-3⟩ are expected to occur most rarely (each of them only in 1 of $3^3 = 27$ cases), whereas the rank-order triplet ⟨1-2-3⟩ is expected to occur most often (in 6 of 27 cases). The resulting chance level for each rank-order triplet is indicated by a gray dashed line. Average rank-order triplets ⟨1-1-1⟩, ⟨2-2-2⟩, and ⟨3-3-3⟩ occurred significantly more often than expected by chance (χ^2 test, $P < 0.001$).

Table 1. *Distribution of response maxima and minima for the simulated eye-movement conditions*

	Leftward	Straight Ahead	Rightward
Monkey H (left hemisphere)			
No. of maximum responses	19	11	60
No. of minimum responses	42	28	20
Monkey C (right hemisphere)			
No. of maximum responses	37	16	1
No. of minimum responses	11	12	31

Recordings were performed in the left hemisphere of *monkey H* and the right hemisphere of *monkey C*. Numerical values indicate the no. of neurons for which in 1 of the 3 simulated eye-movement conditions response maxima and minima were found for leftward, straight-ahead, and rightward self-motion. In both monkeys, heading preference was biased toward the contraversive side (leftward heading for recordings from a right hemisphere, and vice versa).

ances were found in (32 + 29 + 24)/144 = 85/144 = 59% of the cases, i.e., significantly more often than would have been expected (3 × 3.7% = 16/144), if the responses for a given heading direction across the three different eye-movement conditions had been independent (null hypothesis; $\chi^2 = 72.6$, 1 df, $P < 0.001$). This finding was obtained for each of the two experimental animals: in *monkey H*, invariant responses were found in 46/90 = 51% of the cases ($\chi^2 = 33.6$, 1 df, $P < 0.001$), and *in monkey C* in 39/54 = 72% of the cases ($\chi^2 = 41.5$, 1 df, $P < 0.001$).

In the single-cell example shown above (Fig. 2), responses for leftward heading were strongest for all three simulated eye-movement conditions. This cell was recorded in *monkey C*, i.e., from a right hemisphere. Such a maximum response for contraversive heading (i.e., leftward heading for a recording from a right hemisphere and vice versa) was representative of the population of neurons, as shown in Table 1. In both monkeys, this relationship was found for approximately two-thirds of the cases (*monkey H*: 60/90 = 66%; *monkey C*: 37/54 = 69%) and therefore was found significantly more often than would have been expected if maximum responses were distributed at random, i.e., in one-third of the cases (*monkey H*: $\chi^2 = 20.0$, 1 df, $P < 0.001$; *monkey C*: $\chi^2 = 14.8$, 1 df, $P < 0.001$). In a second step of our population analysis, we computed the average discharge values for the three heading directions. When discharges were considered from each animal individually, median responses were strongest for contraversive heading in all eye-movement conditions (repeated-measures ANOVA on ranks, 2 df; *monkey H*: gain = 1.0, $P < 0.001$; gain = 0.5, $P = 0.028$; gain = 0.0, $P = 0.015$; *monkey C*: gain = 1.0, $P = 0.002$; gain = 0.5, $P = 0.002$; gain = 0.0, $P = 0.002$). In all except one case (*monkey H*, gain = 0.5), the weakest median responses were obtained for ipsiversive heading. When responses were considered from both animals for an absolute heading direction (left, straight ahead, and right) rather than ipsiversive vs. contraversive, however, responses for the three heading directions were not significantly different (repeated-measures ANOVA on ranks, 2 df; gain = 1.0, $P = 0.483$; gain = 0.5, $P = 0.704$; gain = 0.0, $P = 0.939$).

As mentioned above, the ranking procedure was based on the complete response interval, i.e., 2,500 ms. In everyday life, 2,500 ms is a rather long time span when it comes to the sensory-based control of self-motion. This consideration almost automatically leads to the question if eye-movement invariant heading responses require the full 2,500 ms to build up. If this were the case, its functional role in sensory-based navigation could be questioned. Hence, we aimed to determine the temporal evolution of the rank-order distribution as shown in Fig. 3. We computed the average activity in increasingly longer temporal intervals (in 50-ms steps) for the baseline period (stationary ground stimulus) and during simulated self-motion. The results are shown in Table 2 and Fig. 4. Table 2 indicates the distribution of rank-order triplets at the end of the baseline period, i.e., while the monkeys fixated a central target during presentation of a stationary ground-plane stimulus. The observed distribution comes close to an expected distribution of a random sample, i.e., when discharges across conditions are not functionally related to each other as is the case during presentation of a stationary stimulus. Figure 4 illustrates how fast this distribution approached the final distribution resulting from eye-movement invariances. Figure 4*A* uses a color code to depict the observed proportion of each of the 10 rank-order triplets. Starting with stimulus-motion onset ($t = 0$ ms), the proportion of the rank-order triplets ⟨1-1-1⟩, ⟨2-2-2⟩, and ⟨3-3-3⟩ rose fast toward their individual saturation values. At the same time, the rank-order triplet ⟨1-2-3⟩, which indicates the highest amount of stimulus-response variance across eye-movement conditions, dropped from chance level to its rather low saturation value. For the two most important rank-order triplets, i.e., the one representing the strongest response (⟨1-1-1⟩) and the one representing the most pronounced variance across eye-movement conditions (⟨1-2-3⟩), we wanted to quantify this temporal evolution in greater detail. We fitted exponential functions [⟨1-1-1⟩: $y = a + b \times (1 - e^{-t/\tau})$; ⟨1-2-3⟩: $y = a + b \times e^{-t/\tau}$] to the observed proportions, which allowed to determine the time constants of the exponential rise (⟨1-1-1⟩) or decline (⟨1-2-3⟩). Both time constants were in the order of $\tau = 400$ ms: $\tau_{\langle 1\text{-}1\text{-}1\rangle} = 438.2$ ms, and $\tau_{\langle 1\text{-}2\text{-}3\rangle} = 380.4$ ms.

Our analysis did not consider a putative neural basis of perceived heading and its modulation by simulated eye movements so far. For two-dimensional visual motion stimuli, a winner-take-all rule explains well monkeys' perception (Salz-

Table 2. *Distribution of rank-order triplets in the baseline period*

	Rank-Order Triplet									
	1-1-1	3-3-3	2-2-2	1-1-2	1-2-2	2-2-3	2-3-3	1-1-3	1-3-3	1-2-3
Expected proportion, %	3.7	3.7	3.7	11.1	11.1	11.1	11.1	11.1	11.1	22.2
Observed proportion, %	3.5	2.1	2.1	9.0	16.0	9.7	15.3	13.2	11.1	18.1

If heading responses across eye movements were completely unrelated, one would expect a random distribution, with rank-order triplets ⟨1-1-1⟩, ⟨2-2-2⟩, and ⟨3-3-3⟩ to be found most rarely and rank-order triplet ⟨1-2-3⟩ to be found most often. The exact values (in %) of such a random distribution are shown as the expected proportion. As expected, the observed distribution of rank-order triplets at the end of the baseline period ($t = 0$), i.e., without a moving stimulus, came very close to this random distribution.

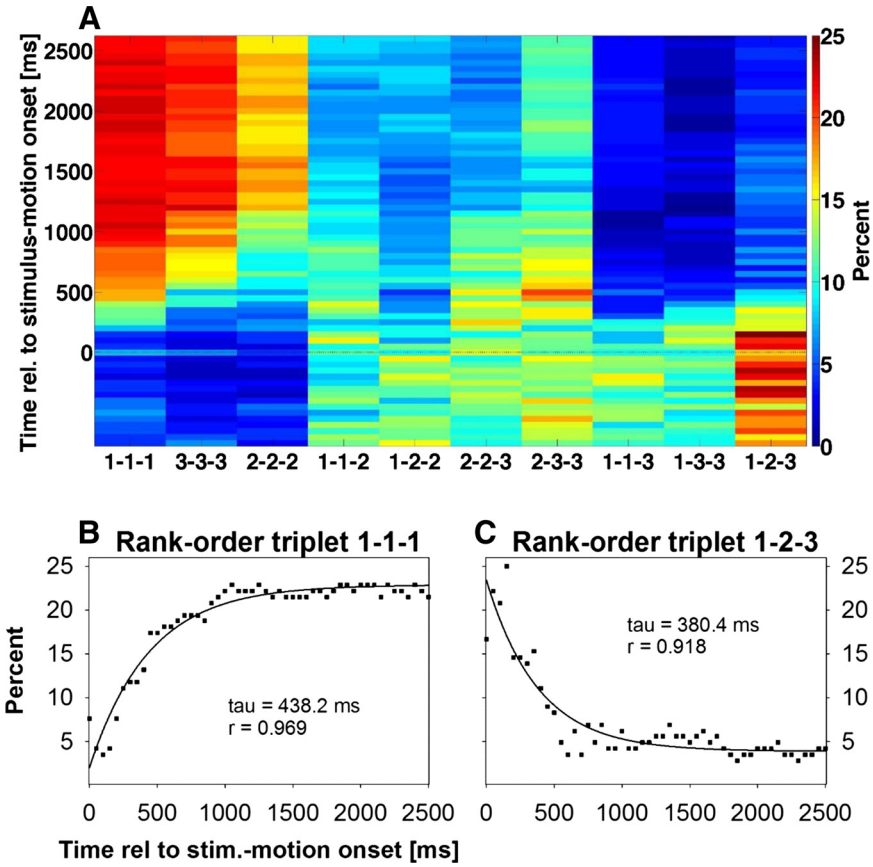

Fig. 4. Temporal development of the rank-order triplets. We computed the average activity in increasingly longer temporal intervals (in 50-ms steps) for the baseline period ($t < 0$ ms) and during simulated self-motion ($t \geq 0$ ms). With the use of a color code, *A* depicts the temporal development of the observed proportion of each of the 10 rank-order triplets. Starting with stimulus-motion onset ($t = 0$ ms), the proportion of the rank-order triplets ⟨1-1-1⟩, ⟨2-2-2⟩, and ⟨3-3-3⟩, which indicate eye-movement invariance of the strongest (⟨1-1-1⟩), medium (⟨2-2-2⟩), and weakest responses (⟨3-3-3⟩), rose fast toward their individual saturation values. The rank-order triplet ⟨1-2-3⟩, which indicates the highest amount of stimulus-response variance across eye-movement conditions, also dropped very fast from chance level to its rather low saturation value. To quantify these temporal developments in greater detail, we fitted exponential functions to the rank-order triplet ⟨1-1-1⟩ (*B*) and ⟨1-2-3⟩ (*C*). Time constants were $\tau_{\langle 1\text{-}1\text{-}1\rangle} = 438.2$ ms and $\tau_{\langle 1\text{-}2\text{-}3\rangle} = 380.4$ ms.

man and Newsome 1994). We determined each neuron's heading preference (i.e., its strongest discharge) during simulated gain = 0.0 and asked how stable this preference was for the other two eye-movement conditions. As an example, a hypothetical neuron might have preferred heading to the right. For the other two eye-movement conditions, preferred heading might also have been to the right (change in preferred heading $d\alpha = 0°$) or straight ahead ($d\alpha = -30°$) or to the left ($d\alpha = -60°$). If heading preferences had not been related to each other across eye-movement conditions, one would have expected the same number of cases (i.e., neurons) for each of the three change directions $d\alpha$, i.e., 0°, −30°, and −60°, respectively. The same thought experiment applies to neurons whose preferred self-motion during gain = 0.0 was straight ahead or to the left. In the first case, possible change directions were $d\alpha = -30°$, 0°, and +30°, whereas in the latter case, these were $d\alpha = 0°$, +30°, and +60°, respectively. In all cases, unrelated heading responses across eye-movement conditions would have resulted in an equal number of neurons for each of the change directions $d\alpha$. The observed distributions of $d\alpha$ were quite different from a uniform distribution and are shown in Table 3, which depicts data from both monkeys as well as from *monkey H* (left hemisphere) and *monkey C* (right hemisphere) individually. Considering data from both monkeys, preferred heading for gain = 0.0 and 0.5 was constant ($d\alpha = 0°$) for 34/48 = 71% of the neurons, i.e., significantly more often than would have been expected by chance ($\chi^2 = 28.3$, 1 df, $P < 0.001$). For gain = 0.0 and 1.0, this proportion was even higher, i.e., it was found for 40/48 = 83% of the neurons ($\chi^2 = 50.5$, 1 df, $P < 0.001$). Also, the preference for contraversive heading was preserved across eye movements (Table 3): in *monkey H*, a shift of strongest discharges from contra- toward ipsiversive heading ($d\alpha = -60°$) as induced by simulated eye movements was found only in 2/20 = 10% of the neurons for gains = 0.0 and 0.5. This value was significantly smaller than expected by chance ($\chi^2 = 16.0$, 1 df, $P < 0.001$). In the same animal, no such shift was found for a comparison of heading preferences between responses during gains = 0.0 and 1.0. In the second animal, not a single shift from contra- to ipsiversive preference ($d\alpha = +60°$) was found.

In both monkeys, preference for straight-ahead motion was underrepresented. We found it only in 9/49 = 19% of the neurons, less often than expected by chance ($\chi^2 = 5.3$, 1 df, $P < 0.05$). The preference for straight-ahead motion appeared less stable across eye-movement conditions than the peripheral preferences. For those nine neurons with a preference for straight-ahead self-motion at gain = 0.0, four (4/9) kept their selectivity at gain = 0.5 and six (6/9) at gain = 1.0. These values were statistically not different from a random distribution, i.e., an equal number of neurons per change direction $d\alpha$ (Fisher exact test: gain = 0.5, $P > 0.3$; gain = 1.0, $P > 0.1$).

In a fourth experimental condition, real eye movements were induced in blocks of trials by removing the fixation target and allowing the animal to freely move its eyes. In this situation, monkeys (as well as other primates) perform spontaneous eye movements that often follow the visual motion experienced along the direction of gaze (Lappe et al. 1998). These spontaneous tracking eye movements are regularly interrupted by resetting fast phases, called saccades in the following for the sake of simplicity. Resulting eye movements for the three

Table 3. *Modulation of heading preference as a function of simulated eye-movement gain*

Heading Preference at $G = 0.0$	Simulated Gains	Change of Heading Preference, dα/deg				
		−60° ←	−30° ←	0°	→ +30°	→ +60°
		Data from both monkeys (n = 48)				
Right	0.0 vs. 0.5	2	4	14		
	0.0 vs. 1.0	0	1	19		
Straight ahead	0.0 vs. 0.5		2	4	3	
	0.0 vs. 1.0		2	6	1	
Left	0.0 vs. 0.5			16	1	2
	0.0 vs. 1.0			15	2	2
Total	0.0 vs. 0.5	2	6	34	4	2
	0.0 vs. 1.0	0	3	40	3	2
		Data from monkey H (n = 30, left hemisphere)				
Right	0.0 vs. 0.5	2	4	14		
	0.0 vs. 1.0	0	1	19		
Straight ahead	0.0 vs. 0.5		0	1	2	
	0.0 vs. 1.0		1	1	1	
Left	0.0 vs. 0.5			5	0	2
	0.0 vs. 1.0			4	1	2
Total	0.0 vs. 0.5	2	4	20	2	2
	0.0 vs. 1.0	0	2	24	2	2
		Data from monkey C (n = 18, right hemisphere)				
Right	0.0 vs. 0.5	0	0	0		
	0.0 vs. 1.0	0	0	0		
Straight-ahead	0.0 vs. 0.5		2	3	1	
	0.0 vs. 1.0		1	5	0	
Left	0.0 vs. 0.5			11	1	0
	0.0 vs. 1.0			11	1	0
Total	0.0 vs. 0.5	0	2	14	2	0
	0.0 vs. 1.0	0	1	16	1	0

We determined each neuron's heading preference, i.e., its strongest discharge, during simulated gain (G) = 0.0 and asked how stable this preference was for the other two eye-movement conditions. Unrelated heading responses across eye-movement conditions would have resulted in an equal number of neurons for each of the change directions dα. The observed distributions of dα were quite different from a uniform distribution. Data from both monkeys, as well as data from *monkey H* (left hemisphere) and *monkey C* (right hemisphere), are shown. For details see main text.

different heading directions, which were recorded together with neuronal activity, are shown in the *middle* and *bottom* rows of Fig. 5. They were mostly horizontal and consistent with the prevalent motion direction on the screen, i.e., rightward slow eye movements for leftward heading, and vice versa. For straight-ahead self-motion, horizontal eye movements were typically very small, thereby consistent with the horizontal flow of the visual stimulus around the screen center. For the analysis of the neuronal firing rate, we considered only the intervals of tracking eye movements between two successive saccades. To this end, all intervals were aligned to the offset of the preceding saccade. Discharges resulting from the neuron whose discharges during simulated eye movements were shown in Fig. 2 are shown in the *top* row of Fig. 5. As can be easily seen, also during free eye movements, the neuron had a strong preference for leftward heading. In other words, this neuron favored a single heading in all four (simulated and real) eye-movement conditions; i.e., it responded in all cases invariantly to the direction of self-motion.

We also ranked the responses during real eye movements. For this neuron, the ranks for leftward, straight-ahead, and rightward heading were ⟨1⟩, ⟨2⟩, and ⟨3⟩, respectively. This rank was combined with the rank-order triplet from the simulated eye-movement condition, resulting in the rank-order quadruplet ⟨1-1-1-1⟩ for leftward heading, ⟨2-2-2-2⟩ for straight-ahead motion, and ⟨3-3-3-3⟩ for rightward heading. Thirty-seven neurons (20 in *monkey H* and 17 in *monkey C*) could be recorded long enough and were tested in the simulated and the real eye-movement conditions (Fig. 6). For each heading direction (left, straight-ahead, and right) tested in each neuron, a single rank-order quadruplet was computed as described above ($n = 3 \times 37 = 111$). A coincidence of heading preferences for simulated and real eye movements (⟨1-1-1-1⟩) was observed in 16 of these 111 cases (13%), i.e., significantly more often than would have been observed if responses across eye-movement conditions had been independent (chance level: 111/81 ~ 1%; $\chi^2 = 14.3$, 1 df, $P < 0.001$). Also, the weakest response (rank-order quadruplet ⟨3-3-3-3⟩), which was observed in 18/111 = 16% of the cases ($\chi^2 = 16.6$, 1 df, $P < 0.001$), and the medium responses (⟨2-2-2-2⟩), observed in 10/111 = 9% of the cases ($\chi^2 = 7.7$, 1 df, $P < 0.01$), occurred more often than would have been expected if responses across eye movements had been independent.

Eye movements induce predictable distortions of the retinal image. Also, from a system's theoretic point of view, visual consequences of real eye movements are predictable by means of efference copy or corollary discharge signals (Sperry 1950; von Holst and Mittelstaedt 1950). These signals could be used to obtain a net signal of optic flow as induced purely by self-motion. Such a compensatory mechanism, however, is not possible for simulated eye movements, for which distortions are not predictable. Hence, we were interested in whether we could find any evidence for reafferent signals during real eye movements and (if so) how they would be represented at the neural level. In other words, we asked whether or not neuronal discharges would differ for real and simulated eye movements. As a first step, we determined for each of the three heading directions the median firing rates as obtained in the four different eye-movement conditions. Remarkably, in most of the cases, discharge values did not differ significantly across eye movements. For leftward and straight-ahead self-motion, discharges across the four eye-movement conditions (simulated eye movements with gain = 0.0, 0.5, and 1.0 and free eye movements) were not significantly different [repeated-measures ANOVA on ranks, 3 df, followed by an all pairwise multiple comparison procedure (Student-Newman-Keuls test): leftward, $P > 0.6$; straight ahead, $P > 0.05$]. For rightward heading, discharges during real eye movements were significantly smaller than during simulated eye movements with gain = 1.0 ($P < 0.05$) and gain = 0.0 ($P < 0.05$). Discharges obtained during free eye movements and simulated eye movements with a gain = 0.5 did not differ significantly ($P > 0.05$).

In a second step of our analysis, we computed for each eye-movement condition the response modulation, i.e., the difference between the maximum (preferred heading) and the minimum response (nonpreferred heading) (Fig. 7). As an example, for the neuron whose discharges are shown in Figs. 2 and 5, these were always the differences between the average discharges for simulated leftward (preferred heading) and rightward (nonpreferred heading) self-motion. For the three different simulated eye movements, these response modulations (RM) were as follows: $RM_{Gain=1.0} = 22.1$ spikes/s, $RM_{Gain=0.5} = 27.7$ spikes/s, and $RM_{Gain=0.0} = 26.2$ spikes/s. For the free eye movements, the response modulation amounted to $RM_{Free} = 20.0$ spikes/s; i.e., RM in the real

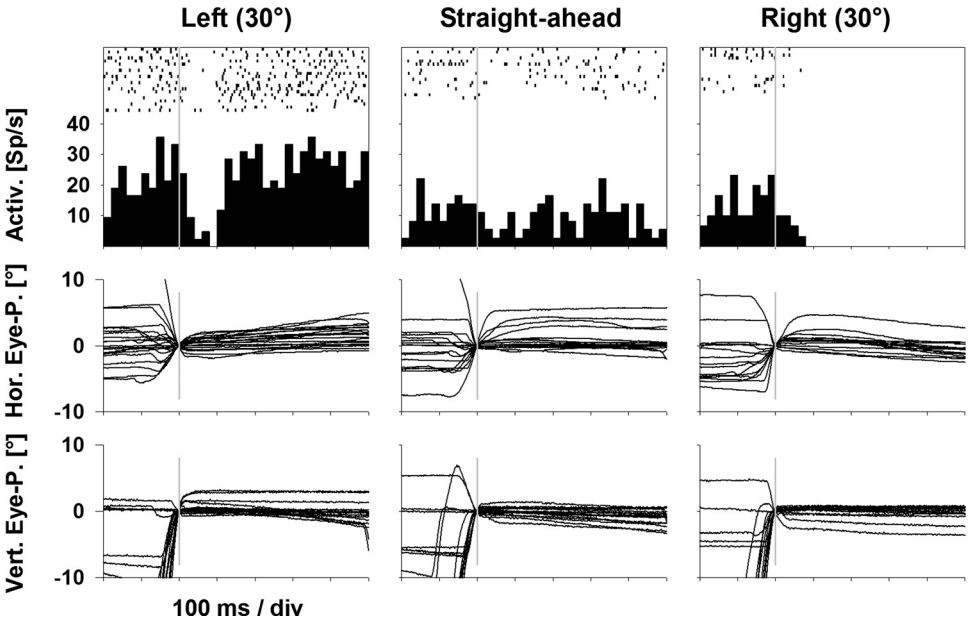

Fig. 5. Self-motion responses during real eye movements. Histograms and spike rasters in *top* row show responses during real eye movements while presenting radial flow on the screen (left, straight ahead, and right). Data stem from the same cell whose discharges during simulated eye movements are shown in Fig. 2. The animal was performing spontaneous tracking eye movements. Because these eye movements add image motion on the retina, the actual retinal motion pattern was similar to the one in Fig. 2 with gain = 0.5. *Middle* and *bottom* rows show horizontal (Hor.) and vertical (Vert.) eye-movement traces of the animal. Neural activity and eye-movement traces are aligned to the offset of the fast phase of the optokinetic-like eye-movement pattern as indicated by the vertical gray lines. Note that the timescales of Figs. 2 and 5 are different. Also, in this free eye-movement condition, the neuron preferred leftward self-motion.

eye-movement condition was smaller than in any of the simulated eye-movement conditions. For the population of neurons ($n = 37$), a statistical test revealed that RM during free eye movements was significantly smaller than RM in any of the simulated eye movements [repeated-measures ANOVA on ranks, 3 df, followed by an all pairwise multiple comparison procedure (Student-Newman-Keuls test), $P < 0.05$], whereas none of the RM values during simulated eye movements was significantly different from each other ($P > 0.05$). This latter result underlines our finding of a similarity of self-motion responses in area VIP during different simulated eye movements.

DISCUSSION

We have investigated self-motion responses in macaque area VIP concerning their invariance with respect to eye movements. In 59% of the cases, tuning for optic flow responses was not changed by superimposed simulated or real eye movements. Response modulation during real eye movements was significantly smaller than during simulated eye movements. Our data provide further evidence for the hypothesis that primate area VIP plays an important role in the sensory control of navigation.

Neural basis of eye-movement invariant heading responses. Gibson (1950) proposed that the visual flow in the optic field surrounding a moving observer contained sufficient information to estimate heading just from invariances in the flow pattern itself. His further suggestion, however, that the focus of expansion in the flow is such an invariant is problematic, since in everyday life the optic flow as sensed by the eyes is superimposed with tracking eye movements that distort the flow structure and destroy the focus of expansion (Fig. 1). Such eye movements are reflexively induced by the flow itself and attempt to stabilize the foveal and parafoveal image (Lappe et al. 1998; Wei and Angelaki 2006). Human observers are able to estimate heading from such complex spiraling flow fields in the absence of a focus of expansion (Van den Berg 1993; Warren and Hannon 1988).

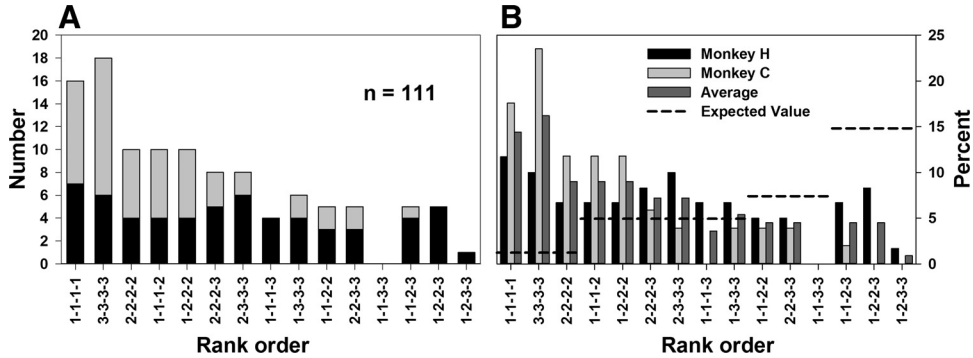

Fig. 6. Distribution of rank-order quadruplets. For each cell, we ranked (from ⟨1⟩ = strongest to ⟨3⟩ = weakest) for each simulated self-motion direction the responses of a neuron for each of the 3 simulated eye-movement conditions and the real eye-movement condition. As an example, for the neuron whose responses are shown in Figs. 2 and 4, rank-order quadruplets for leftward, straight-ahead, and rightward self-motion were ⟨1-1-1-1⟩, ⟨2-2-2-2⟩, and ⟨3-3-3-3⟩, respectively. For the population of neurons ($n = 37$) we obtained $3 \times 37 = 111$ rank-order quadruplets. *A* shows the absolute number of each of the rank-order quadruplets for both monkeys. *B* shows the resulting proportions, for each monkey and as an average. A coincidence of heading preferences for simulated and real eye movements (⟨1-1-1-1⟩) was observed in 16 of 111 cases (13%; chance level: 1%; χ^2 test, 1 df, $P < 0.001$). Also, rank-order quadruplets ⟨3-3-3-3⟩ (18 cases = 16%; χ^2 test, 1 df, $P < 0.001$) and ⟨2-2-2-2⟩ (10 cases = 9%; χ^2 test, 1 df, $P < 0.01$) occurred significantly more often than would have been expected if responses had been independent. Chance levels of individual rank-order quadruplets are indicated by black dashed lines.

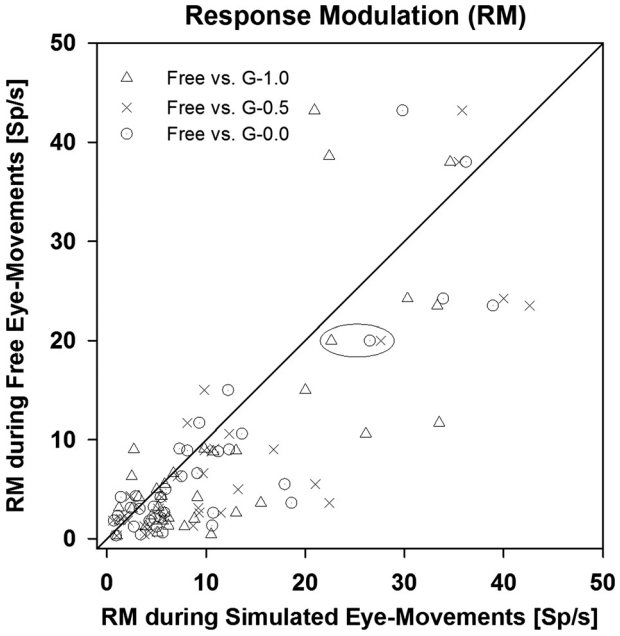

Fig. 7. Response modulation during real and simulated eye movements. During simulated (abscissa) and real (ordinate) eye movements each neuron had a strongest and a weakest response. For each neuron, we computed the difference of these 2 values, defining a response modulation (RM) for each of the 3 eye-movement conditions (symbols: △, gain = 1.0; ×, gain = 0.5; ○, gain = 0.0). At the population level, RM was significantly stronger for each simulated eye-movement condition compared with free eye movements ($n = 37$, repeated-measures ANOVA on ranks, followed by pairwise comparison, $P < 0.05$), whereas none of the RMs during simulated eye movements was significantly different from each other ($P > 0.05$). The 3 symbols surrounded by an ellipsoid indicate the RM values obtained from data in Figs. 2 and 5.

We have used the simulated eye movement technique (Warren and Hannon 1990) to show that VIP neurons respond selectively to heading irrespective of the occurrence of such tracking eye movements. Crucially, this invariant response was derived from purely visual mechanisms. Hence, our findings show that VIP neurons can use visual information from the distorted retinal flow during combined self-motion and tracking eye movements to estimate heading. This ability to cope with distorted flow fields is important because eye movements are common during natural self-motion (Lappe et al. 1998). In principle, there are two possibilities by which the visual system could extract heading when retinal flow is distorted by eye movements: it could either use nonvisual (extraretinal) information about the eye movement, or it could use the distorted structure of the retinal motion pattern itself. The use of extraretinal eye-movement signals to compensate for the distortions that smooth pursuit eye movements introduce in retinal flow has been shown for area VIP (Maciokas and Britten 2010; Zhang and Britten 2011), consistent with similar findings for area MST (Bradley et al. 1996; Upadhyay et al. 2000) and with evidence for the use of such a signal in humans (Lappe et al. 1999; Royden et al. 1992; Warren and Hannon 1990). Humans, however, can also use the structure of the flow pattern directly. This is particularly true for travel over a horizontal ground plane and eye movements that simulate natural gaze stabilization mechanisms (Van den Berg 1993; Warren and Hannon 1988). In this case, the retinal flow pattern has a characteristic spiraling structure (see also Fig. 1). Our results demonstrate that neurons from area VIP can analyze this structure for retaining their heading selectivity during eye movements. Such invariant heading responses require complicated visual tuning of heading detectors. The receptive field structure of VIP neurons is not fully understood but is known to be complex (Chen et al. 2014; Schaafsma and Duysens 1996). The existence of neuronal mechanisms that determine heading visually from distorted flow fields has been proposed in several neural models for heading detection (Beintema and Van den Berg 1998; Lappe and Rauschecker 1993; Perrone and Stone 1994). Curiously, these models share the prediction of a bicircular receptive field (RF) structure (Beintema et al. 2004). It will be interesting to see how the receptive fields of invariant heading detectors in area VIP are structured. Along this research question, Chen et al. (2014) provided first evidence that RF properties might critically depend on the stimulus used to map the RF location.

Recently, by using the exact same set of stimuli, we have shown eye-movement invariant heading responses for neurons in macaque area MST (Bremmer et al. 2010). Remarkably, macaque areas VIP and MST share a number of response features. Most importantly, these are visual and vestibular self-motion responses (Bremmer et al. 1999; Chen et al. 2011b; Duffy 1998; Duffy and Wurtz 1991a; Schlack et al. 2002; Takahashi et al. 2007). Responses from populations of neurons in both areas allow to decode heading in a fixed gaze condition (Bremmer et al. 2002a; Britten 2008; Gu et al. 2010; Lappe et al. 1996). Electrical microstimulation of neurons in both areas changes self-motion perception in monkeys (Britten and van Wezel 1998; Zhang and Britten 2011). Finally, MST and VIP neurons also respond to spiraling motion patterns (Graziano et al. 1994; Schaafsma and Duysens 1996). It was suggested that such sensitivity might be related to a visual mechanism for heading estimation during eye movements that analyzes the distorted structure of the retinal flow induced by tracking eye movements and that functions as a backup for extraretinal processes (Lappe and Rauschecker 1993; Perrone and Stone 1994). The data from our current study on area VIP as well as our data on MST (Bremmer et al. 2010) provide strong evidence in support of this hypothesis.

Time course of heading encoding and its eye-movement invariance. We determined the time course of heading tuning as determined by rank-order triplets. By fitting exponential functions to their temporal evolution we found time constants in the order of $\tau = 400$ ms. This time span fits nicely results from behavioral studies on heading perception. As an example, Grigo and Lappe (1999) tested heading while subjects virtually approached a vertical plane. Accurate judgments were observed when the field of view was large (as was in our case) and the stimulus duration was shorter than 500 ms. For a small field of view or a prolonged stimulus presentation, heading error increased. In another study, Hooge et al. (1999) asked subjects to saccade toward perceived heading in a visual display that mimicked self-motion. These authors found a heading processing time of ~430 ms. Taken together, our results provide neurophysiological support for these behavioral findings.

In a next step we asked if heading could be deduced from our neurophysiological data and how stable this measure would be across eye movements. We assumed that heading might be represented based on a winner-take-all regime (Salzman and Newsome 1994). We found that for 71% (in the one pair of eye

movements) or even 83% of the neurons (for the other pair of eye movements), the strongest heading response was invariant to simulated eye movements. This finding is remarkable since a rather accurate estimate of self-motion direction would already be given by a comparably small number of neurons (n = 48 in our case). This finding required, however, that data from both hemispheres were considered. When taking data from a single hemisphere instead, ipsiversive heading was encoded rarely (in 5/30 neurons in *monkey H*) or not at all (in 0/18 neurons in *monkey C*). In addition, strongest responses for straight-ahead self-motion were found less often and appeared less stable than for leftward or rightward heading. An overrepresentation of peripheral headings over straight-ahead motion is in line with previous studies on self-motion encoding in area MST (e.g., Gu et al. 2010; Lappe et al. 1996) as well as in area VIP (Chen et al. 2011b). A rather speculative prediction resulting from this finding concerns a system with a unilateral damage to optic flow processing. A consequence might be an impairment of the encoding or the sensory control of heading. More specifically, an imbalance between left and right hemispheric optic flow processing might induce an ipsiversive bias (with respect to the lesioned site). Neurological patients suffering from stroke sometimes reveal such a unilateral cerebral lesion (e.g., Vossel et al. 2013). Indeed, there is evidence that patients with a right hemispheric lesion show an ipsiversive deviation from a straight path when walking toward a target in front of them (Turton et al. 2009). We would like to emphasize, however, that this hypothesis is rather speculative and definitely requires more, ideally combined, neurophysiological, behavioral, and neuropsychological approaches.

Reafferent signals and the processing of self-motion responses. In addition to compensatory mechanisms based purely on visual information, we also found evidence for nonvisual or extraretinal signals being involved in self-motion processing. In blocks of trials, monkeys were allowed to freely move their eyes. This resulted typically in reflexive eye movements being composed of slow tracking phases and fast-resetting eye movements. Here, differently from the simulated eye-movement conditions, eye-movement signals in the form of an efference copy or corollary discharge (Sperry 1950; von Holst and Mittelstaedt 1950) were available. Such extraretinal signals are thought to help dissociating self-induced from externally induced motion (Erickson and Thier 1991; Galletti et al. 1990; Sommer and Wurtz 2008). Our results are consistent with a neural signature of such reafferent signaling. Response modulation (RM) between strongest and weakest discharges was smallest for the real eye-movement condition compared with all simulated eye-movement conditions. We suggest that this reduced response modulation would be consistent with reafferent processing of visual motion information: in the simulated eye-movement condition, the response modulation would encode both the eye-movement-induced and the self-motion-induced visual signal. On the contrary, the response modulation in the real eye-movement condition would indicate only the net visual signal resulting from the (simulated) self-motion. Further experiments, however, are needed to test this hypothesis.

GRANTS

This work was supported by Deutsche Forschungsgemeinschaft SFB-TRR-135/A2.

AUTHOR CONTRIBUTIONS

M.L. and F.B. conception and design of research; A.S. and F.B. performed experiments; A.K. and F.B. analyzed data; F.B. interpreted results of experiments; F.B. prepared figures; F.B. drafted manuscript; A.K., K.-P.H., M.L., and F.B. edited and revised manuscript; A.K., A.S., K.-P.H., M.L., and F.B. approved final version of manuscript.

DISCLOSURES

No conflicts of interest, financial or otherwise, are declared by the authors.

REFERENCES

Avillac M, Ben Hamed S, Duhamel JR. Multisensory integration in the ventral intraparietal area of the macaque monkey. *J Neurosci* 27: 1922–1932, 2007.

Avillac M, Deneve S, Olivier E, Pouget A, Duhamel JR. Reference frames for representing visual and tactile locations in parietal cortex. *Nat Neurosci* 8: 941–949, 2005.

Beintema JA, Van den Berg AV. Heading detection using motion templates and eye velocity gain fields. *Vision Res* 38: 2155–2179, 1998.

Beintema JA, Van den Berg AV, Lappe M. Circular receptive field structures for flow analysis and heading detection. In: *The Structure of Receptive Fields for Flow Analysis and Heading Detection*, edited by Vaina LM, Beardsley SA, and Rushton S. Norwell, MA: Kluwer Academic, 2004, p. 223–248.

Ben Hamed S, Duhamel JR, Bremmer F, Graf W. Visual receptive field modulation in the lateral intraparietal area during attentive fixation and free gaze. *Cereb Cortex* 12: 234–245, 2002.

Bradley DC, Maxwell M, Andersen RA, Banks MS, Shenoy KV. Mechanisms of heading perception in primate visual cortex. *Science* 273: 1544–1547, 1996.

Bremmer F, Duhamel JR, Ben Hamed S, Graf W. Heading encoding in the macaque ventral intraparietal area (VIP). *Eur J Neurosci* 16: 1554–1568, 2002a.

Bremmer F, Klam F, Duhamel JR, Ben Hamed S, Graf W. Visual-vestibular interactive responses in the macaque ventral intraparietal area (VIP). *Eur J Neurosci* 16: 1569–1586, 2002b.

Bremmer F, Kubischik M, Hoffmann KP, Krekelberg B. Neural dynamics of saccadic suppression. *J Neurosci* 29: 12374–12383, 2009.

Bremmer F, Kubischik M, Pekel M, Hoffmann KP, Lappe M. Visual selectivity for heading in monkey area MST. *Exp Brain Res* 200: 51–60, 2010.

Bremmer F, Kubischik M, Pekel M, Lappe M, Hoffmann KP. Linear vestibular self-motion signals in monkey medial superior temporal area. *Ann NY Acad Sci* 871: 272–281, 1999.

Britten KH. Mechanisms of self-motion perception. *Annu Rev Neurosci* 31: 389–410, 2008.

Britten KH, van Wezel RJ. Electrical microstimulation of cortical area MST biases heading perception in monkeys. *Nat Neurosci* 1: 59–64, 1998.

Chen A, DeAngelis GC, Angelaki DE. A comparison of vestibular spatiotemporal tuning in macaque parietoinsular vestibular cortex, ventral intraparietal area, and medial superior temporal area. *J Neurosci* 31: 3082–3094, 2011a.

Chen A, DeAngelis GC, Angelaki DE. Representation of vestibular and visual cues to self-motion in ventral intraparietal cortex. *J Neurosci* 31: 12036–12052, 2011b.

Chen X, DeAngelis GC, Angelaki DE. Eye-centered visual receptive fields in the ventral intraparietal area. *J Neurophysiol* 112: 353–361, 2014.

Colby CL, Duhamel JR, Goldberg ME. Ventral intraparietal area of the macaque: anatomic location and visual response properties. *J Neurophysiol* 69: 902–914, 1993.

Duffy CJ. MST neurons respond to optic flow and translational movement. *J Neurophysiol* 80: 1816–1827, 1998.

Duffy CJ, Wurtz RH. Sensitivity of MST neurons to optic flow stimuli. I. A continuum of response selectivity to large-field stimuli. *J Neurophysiol* 65: 1329–1345, 1991a.

Duffy CJ, Wurtz RH. Sensitivity of MST neurons to optic flow stimuli. II. Mechanisms of response selectivity revealed by small-field stimuli. *J Neurophysiol* 65: 1346–1359, 1991b.

Duhamel JR, Colby CL, Goldberg ME. Ventral intraparietal area of the macaque: congruent visual and somatic response properties. *J Neurophysiol* 79: 126–136, 1998.

Erickson RG, Thier P. A neuronal correlate of spatial stability during periods of self-induced visual motion. *Exp Brain Res* 86: 608–616, 1991.

Galletti C, Battaglini PP, Fattori P. 'Real-motion' cells in area V3A of macaque visual cortex. *Exp Brain Res* 82: 67–76, 1990.

Gibson JJ. The perception of the visual world. *Boston*: Houghton Mifflin, 1950.

Graziano MS, Andersen RA, Snowden RJ. Tuning of MST neurons to spiral motions. *J Neurosci* 14: 54–67, 1994.

Grigo A, Lappe M. Dynamical use of different sources of information in heading judgments from retinal flow. *J Opt Soc Am A* 16: 2079–2091, 1999.

Gu Y, Angelaki DE, DeAngelis GC. Neural correlates of multisensory cue integration in macaque MSTd. *Nat Neurosci* 11: 1201–1210, 2008.

Gu Y, DeAngelis GC, Angelaki DE. A functional link between area MSTd and heading perception based on vestibular signals. *Nat Neurosci* 10: 1038–1047, 2007.

Gu Y, DeAngelis GC, Angelaki DE. Causal links between dorsal medial superior temporal area neurons and multisensory heading perception. *J Neurosci* 32: 2299–2313, 2012.

Gu Y, Fetsch CR, Adeyemo B, DeAngelis GC, Angelaki DE. Decoding of MSTd population activity accounts for variations in the precision of heading perception. *Neuron* 66: 596–609, 2010.

Hooge IT, Beintema JA, van den Berg AV. Visual search of heading direction. *Exp Brain Res* 129: 615–628, 1999.

Judge SJ, Richmond BJ, Chu FC. Implantation of magnetic search coils for measurement of eye position: an improved method. *Vision Res* 20: 535–538, 1980.

Lappe M, Bremmer F, Pekel M, Thiele A, Hoffmann KP. Optic flow processing in monkey STS: a theoretical and experimental approach. *J Neurosci* 16: 6265–6285, 1996.

Lappe M, Bremmer F, Van den Berg AV. Perception of self-motion from visual flow. *Trends Cogn Sci* 3: 329–336, 1999.

Lappe M, Pekel M, Hoffmann KP. Optokinetic eye movements elicited by radial optic flow in the macaque monkey. *J Neurophysiol* 79: 1461–1480, 1998.

Lappe M, Rauschecker JP. A neural network for the processing of optic flow from ego-motion in man and higher mammals. *Neural Comput* 5: 374–391, 1993.

Lappe M, Rauschecker JP. Heading detection from optic flow. *Nature* 369: 712–713, 1994.

Maciokas JB, Britten KH. Extrastriate area MST and parietal area VIP similarly represent forward headings. *J Neurophysiol* 104: 239–247, 2010.

Morgan ML, DeAngelis GC, Angelaki DE. Multisensory integration in macaque visual cortex depends on cue reliability. *Neuron* 59: 662–673, 2008.

Morris AP, Kubischik M, Hoffmann KP, Krekelberg B, Bremmer F. Dynamics of eye-position signals in the dorsal visual system. *Curr Biol* 22: 173–179, 2012.

Page WK, Duffy CJ. Heading representation in MST: sensory interactions and population encoding. *J Neurophysiol* 89: 1994–2013, 2003.

Perrone JA, Stone LS. A model of self-motion estimation within primate extrastriate visual cortex. *Vision Res* 34: 2917–2938, 1994.

Robinson DA. A method of measuring eye movement using a scleral search coil in a magnetic field. *IEEE Trans Biomed Eng* 10: 137–145, 1963.

Royden CS, Banks MS, Crowell JA. The perception of heading during eye movements. *Nature* 360: 583–585, 1992.

Schaafsma SJ, Duysens J. Neurons in the ventral intraparietal area of awake macaque monkey closely resemble neurons in the dorsal part of the medial superior temporal area in their responses to optic flow patterns. *J Neurophysiol* 76: 4056–4068, 1996.

Schlack A, Hoffmann KP, Bremmer F. Interaction of linear vestibular and visual stimulation in the macaque ventral intraparietal area (VIP). *Eur J Neurosci* 16: 1877–1886, 2002.

Shenoy KV, Bradley DC, Andersen RA. Influence of gaze rotation on the visual response of primate MSTd neurons. *J Neurophysiol* 81: 2764–2786, 1999.

Sommer MA, Wurtz RH. Brain circuits for the internal monitoring of movements. *Annu Rev Neurosci* 31: 317–338, 2008.

Sperry RW. Neural basis of the spontaneous optokinetic response produced by visual inversion. *J Comp Physiol Psychol* 43: 482–489, 1950.

Takahashi K, Gu Y, May PJ, Newlands SD, DeAngelis GC, Angelaki DE. Multimodal coding of three-dimensional rotation and translation in area MSTd: comparison of visual and vestibular selectivity. *J Neurosci* 27: 9742–9756, 2007.

Turton AJ, Dewar SJ, Lievesley A, O'Leary K, Gabb J, Gilchrist ID. Walking and wheelchair navigation in patients with left visual neglect. *Neuropsychol Rehabil* 19: 274–290, 2009.

Upadhyay UD, Page WK, Duffy CJ. MST responses to pursuit across optic flow with motion parallax. *J Neurophysiol* 84: 818–826, 2000.

Van den Berg AV. Perception of heading. *Nature* 365: 497–498, 1993.

von Holst E, Mittelstaedt H. Das Reafferenzprinzip. *Naturwissenschaften* 37: 464–476, 1950.

Vossel S, Weiss PH, Eschenbeck P, Fink GR. Anosognosia, neglect, extinction and lesion site predict impairment of daily living after right- hemispheric stroke. *Cortex* 49: 1782–1789, 2013.

Warren WH, Hannon DJ. Direction of self-motion is perceived from optical flow. *Nature* 336: 162–163, 1988.

Warren WH, Hannon DJ. Eye movements and optical flow. *J Opt Soc Am A* 7: 160–169, 1990.

Wei M, Angelaki DE. Foveal visual strategy during self-motion is independent of spatial attention. *J Neurosci* 26: 564–572, 2006.

Yu CP, Page WK, Gaborski R, Duffy CJ. Receptive field dynamics underlying MST neuronal optic flow selectivity. *J Neurophysiol* 103: 2794–2807, 2010.

Zhang T, Britten KH. Parietal area VIP causally influences heading perception during pursuit eye movements. *J Neurosci* 31: 2569–2575, 2011.

Zhang T, Heuer HW, Britten KH. Parietal area VIP neuronal responses to heading stimuli are encoded in head-centered coordinates. *Neuron* 42: 993–1001, 2004.